Design and Testing of a Radiofrequency Ellipsoidal Helmholtz Coil in Contrast with a Circular Pair for Nuclear Magnetic Resonance

Khalid Al-Snaie
Department of Electrical Engineering, College of Engineering, Imam Mohammad Ibn Saud Islamic University, Saudi Arabia
kalsnaie@imamu.edu.sa (corresponding author)

Received: 11 April 2023 | Revised: 27 April 2023 | Accepted: 5 May 2023

 DOI: https://doi.org/10.48084/etasr.5945

ABSTRACT

The design and testing of a Helmholtz prototype probe with a relatively homogeneous radiofrequency field that can be used for MRI are presented in this paper. It consists of two coaxial separately tuned ellipsoidal rings of wire in a symmetric arrangement. The developed ellipsoidal structure is tested experimentally in free space and is compared with the results obtained with an equivalent circular standard Helmholtz coil. Complete electrical modeling of the coils taking into account all couplings (inductive and capacitive) is studied. The proposed ellipsoidal Helmholtz coil provides better performance in terms of field homogeneity, efficiency, and quality factor. The width of the lobe at 10% for the ellipsoidal coil is 20% bigger. Moreover, a significant improvement in the quality factor is observed in free space. Also, the efficiency is increased by 37%. Finally, the Signal to Noise Ratio (SNR) of the ellipsoidal coil is higher than that of the circular coil.

Keywords-MRI; NMR; radio frequency; RF coil; ellipsoidal configuration; B_1 homogeneity

I. INTRODUCTION

Magnetic Resonance Imaging (MRI) is a non-invasive imaging technique that does not use harmful radiation, unlike other imaging modalities. MRI is based on the phenomenon of Nuclear Magnetic Resonance (NMR), a phenomenon independently discovered by two research teams [1, 2]. NMR exploits the resonant behavior exhibited by certain materials when placed in a strong magnetic field. These materials selectively absorb electromagnetic energy at a frequency specific to their constituent cores and which varies with the strength of the externally applied static magnetic field. The absorption of electromagnetic energy positions moves the nuclei of the materials in a state of resonance, after which they return to their original state of thermodynamic equilibrium through a process known as relaxation with release of energy. In addition, there are a host of tissue-specific properties that interact with applied magnetic fields, the two most important of which are relaxation longitudinal (spin-lattice) and transverse relaxation mechanisms (spin-lattice). The use of signal coding techniques based on a spatial arrangement of magnetic field gradients allows obtaining information on the internal structure of biological samples. This information carried by the energy emitted by biological tissues, constitutes the basis of the MRI imaging modality [3-5].

In MRI, the need to make coils with the most uniform radiofrequency (RF) field B_1 is necessary, hence the use of volume RF coils. Among these volume coils, there are the "birdcage" type coils, with several types of operation and structures. They give good results, but they still have some drawbacks and constraints related to their construction. Indeed, the realization of this type of coils becomes complex because the most homogeneous RF field is obtained with a high number of bars, moreover, the excessive metal mass constituting the base rings of the coils loops out to be a seat of Foucault induced currents and causes disturbances during the switching of the gradients and visible trailing phenomena on the images. Moreover, the homogeneity of the B_1 field and the quality factor depend on the symmetry of the coil, hence the need for more precision at the manufacturing level [6-8].

In the case of simpler coils, such as Helmholtz coils which generate a field B_1 along the axis of the coil, the improvement in the homogeneity of the field is clearly greater. Thus, unlike "birdcage" type coils, the optimization of the structure in the absence of periodicity is very significant [7-9].

The main objective of this paper is the design and testing of circular and ellipsoidal Helmholtz coils that can produce a relatively, high electromagnetic field homogeneity to be used for NMR applications.

II. CALCULATION OF THE B_1 MAGNETIC FIELD

This section is devoted to the calculation of the field produced by the circular and ellipsoidal structures. The objective is to obtain an RF induction B_1 of better homogeneity so as to produce a homogeneous field of order 2 in the optimum case. The structure has a reduced dimension compared to the wavelength, so it is possible to apply the law of Biot-Savart and the principle of superposition to obtain the total field [9] on their axis [10]. The magnetic field of a circular loop of N turns whose plane of the coil is centered at $z=+R/2$ (field $B_1(z)$), is written [11-12] as:

$$B_1(z) = \frac{\mu_0 n I R^2}{2\left(R^2+\left(z-\frac{R}{2}\right)^2\right)^{\frac{3}{2}}} \quad (1)$$

while the magnetic field of a loop of N turns whose plane of the coil is centered at $y= -R/2$ (field $B_2(z)$), is:

$$B_2(z) = \frac{\mu_0 n I R^2}{2\left(R^2+\left(z+\frac{R}{2}\right)^2\right)^{\frac{3}{2}}} \quad (2)$$

The field on the axis of a circular Helmholtz coil is the combination of the two previous magnetic fields, the superposition theorem which is validated by the linearity of Maxwell's equations gives the total field:

$$B_{\text{Helmholtz}}(z) = B_1(z) + B_2(z) \quad (3)$$

We proceed by similarity with a structure consisting of two ellipsoidal loops, as shown in Figure 1. Each single loop has a semi-axial dimension x_1 and y_1.

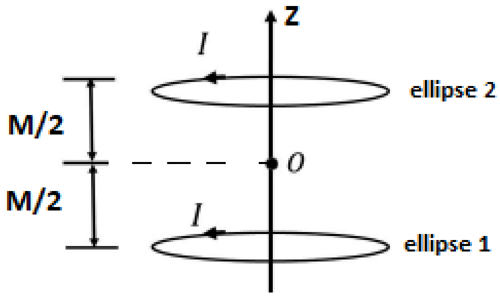

Fig. 1. Helmholtz structure with elliptic loops.

To analyze this situation, a formula for the field produced around the origin ($x = y = z = 0$) by any loop traversed by a current I and of declination α with respect to Oz is proposed [13-14]:

$$B_{1z} = \left(\frac{i\mu_0}{2} f\right) \sin\alpha \times \left\{\sum_{n=0}^{n=\infty} P_{n+1,1}(\cos\alpha)\left(\frac{r}{f}\right)^n P_n(\cos\theta)\right\} \quad (4)$$

where $P_{nm}(\cos\alpha)$ are the associated Legendre polynomials and $P_n(\cos\alpha)$ are the Legendre polynomials.

For the field on the O_z axis, $P_n(\cos\theta) = 1$, and $r = z$, and the previous equation becomes:

$$B_{1z} = \left(\frac{i\mu_0}{2} f\right) \sin\alpha \left\{\sum_{n=0}^{n=\infty} P_{n+1,1}(\cos\alpha)\left(\frac{z}{f}\right)^n\right\} \quad (5)$$

The total field is the sum of the elementary inductions. It is possible to use the first terms of development. Thus an appropriate spacing of the two loops allows a better homogeneity of the magnetic field with a cancellation of derivatives of order two of the field B_1 along the axis Oz and fortuitously the derivative of order four is relatively weak. For this, the two loops must be positioned at an azimuthal angle α of 0.734 rad (about 42°). There is a unique solution for which the second order derivative of the field B_1 is zero. For this optimal structure (E_{opt}), the secondary geometric data are shown in Table I.

TABLE I. PARAMETERS OF THE ELLIPSOIDAL COIL

Primary axis a (cm)	Secondary axis b (cm)	α (rad/deg)
3.042	2.459	0.734/42.09

The eccentricity of the ellipsoid is:

$$e = \sqrt{1-\left(\frac{b^2}{a^2}\right)} = 0.587 \quad (6)$$

The value of the magnetic field at any point in the space is the sum of the fields created at this point by each of the single ellipsoidal loops and the approximated expression is [15-16]:

$$B_z = \frac{\mu_0 I a b}{\pi}\left\{\frac{E\left(\frac{a^2-b^2}{a^2+(M-z)^2}\right)}{(b^2+(M-z)^2)\sqrt{a^2+(M-z)^2}} + \frac{E\left(\frac{a^2-b^2}{a^2+(M+z)^2}\right)}{(b^2+(M+z)^2)\sqrt{a^2+(M+z)^2}}\right\} \quad (7)$$

with:

$$E(k) = \int_0^{\frac{\pi}{2}} \sqrt{1-k^2\sin^2\theta}\, d\theta \quad (8)$$

III. COMPARISON OF THE B_1 FIELD HOMOGENEITY

The performance in terms of homogeneity of the B_1 field of the ellipsoidal Helmholtz Coil (H_E) are compared with a circular Helmholtz Coil (H_C) of the same radial size (diameter d equal to 5cm). Figure 2 shows the simulation of the theoretical curves of the normalized magnetic induction B_{1z} produced along the axis Oz by both coils.

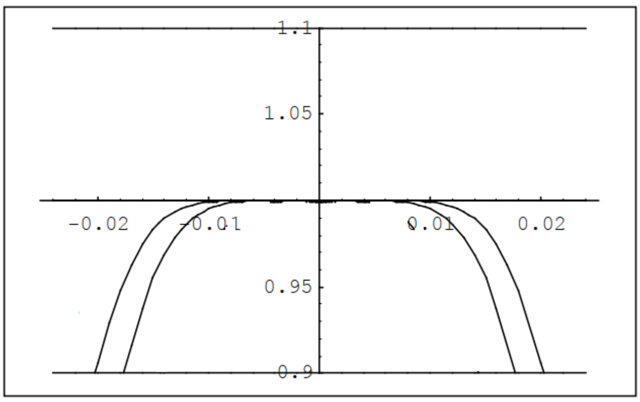

Fig. 2. Profiles along the Oz axis (in m) of the normalized induction (coils: H_C, H_E).

Thus, the theoretical width (absolute or relative) of the profiles can be calculated at 1% and 10% of the maximum. The values are presented in Table II.

TABLE II. PROFILE WIDTH FOR BOTH COILS

Configuration	Profile width at 1%	Profile width at 10%
Circular H_C	2.31	3.83
Ellipsoidal H_E	2.92	4.44

Compared to the reference H_C, the lobe width at 10% of the ellipsoidal coil is increased by 12%. This increase is also greater (20%) for lobe width at 1%. The performance stated above is very general and does not in fact depend on the size of the coil. Indeed, it suffices to apply a simple scale factor compared to the circular and ellipsoidal prototypes to obtain coils of greater or lesser size.

IV. ELECTRICAL MODELING

In this section, the complete electrical modeling of the structures, considering all couplings, is investigated. The complete electrical modeling of the coils is necessary to explain their operation and thereby demonstrate their feasibility. The general electrical model for the developed structures is represented schematically in Figure 3.

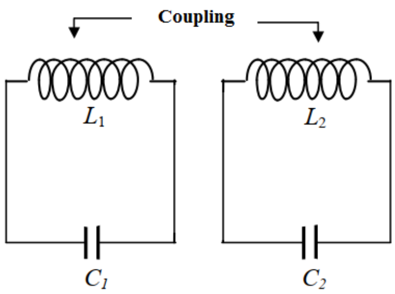

Fig. 3. General electrical model for the developed structures.

Because of the symmetry, the input impedance Z can be expressed as [17-19]:

$$\left.\begin{array}{l} Z_1 = JL_1\omega + \frac{1}{jC_1\omega} + jM_{12}\omega \\ Z_2 = JL_2\omega + \frac{1}{jC_2\omega} + jM_{12}\omega \end{array}\right\} \tag{9}$$

The two electrically isolated loops are characterized by a set of two equations with two unknowns (I_1 and I_2):

$$\begin{pmatrix} z & J(M_{1\,2})\omega \\ J(M_{1\,2})\omega & z \end{pmatrix} \binom{I_1}{I_2} = \binom{0}{0} \tag{10}$$

In fact, two resonance modes are distinguished: a co-current mode with a symmetric behaviour $I_1 = I_2$, which is the mode of interest, and a counter-current mode with non-symmetric behaviour $I_1 = -I_2$ (gradient mode). In co-current mode, the system of (10) comes down to a single equation [20]:

$$ZI_1 + J(M_{1\,2})\omega I_2 = 0 \tag{11}$$

Equation (10) corresponds to the resonance equation:

$$(L_1 + M_{12})\omega^2 - \frac{1}{C} = 0 \tag{12}$$

If the coupling coefficient k is introduced ($M_{12} = k\, L_1$), the resonance equation (12) becomes:

$$C\left(L_1 + k_{12}\sqrt{L_1L_2}\right)\omega^2 = 1 \tag{13}$$

Equation (13) has a positive real solution [21]:

$$f_1 = \frac{1}{2\pi\sqrt{C(L_1 + k_{12}\sqrt{L_1L_2})}} \tag{14}$$

For the counter-current mode ($I_1 = -I_2$), the value of frequency is:

$$f_2 = \frac{1}{2\pi\sqrt{C(L_1 - k_{12}\sqrt{L_1L_2})}} \tag{15}$$

The two resonance modes are located on either side of the resonance frequency f_0 ($f_0 = 1/(LC)$ and they are all the more distant as the coupling is strong. A representation of the input impedance amplitude Z_e is given in Figure 4.

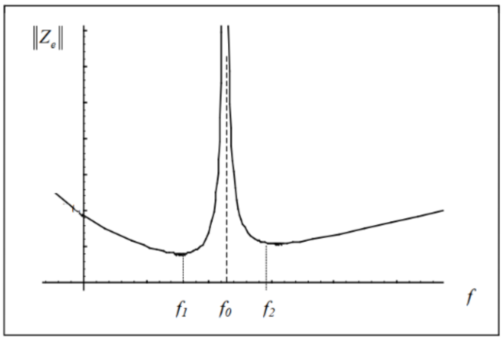

Fig. 4. Theoretical curve of the input impedance of two identical tuned circuits.

The current ratio is given by the secondary circuit equation, which is [22]:

$$\frac{I_1}{I_2} = \frac{-jM\omega}{Z} \tag{16}$$

When there are no losses at the resonance frequency f_1 of the first mode Z=jX=−j$M\omega$ and consequently I_2/I_1=+1, the mode is co-current.

For the mode at frequency f_2, a change of sign takes place, so Z = jX = + j$M\omega$ and the mode is counter current ($I_2/I_1 = -1$).

In the case of low losses or high quality factor, i.e. $Q_0 = RL\omega_0 >> 1$ [23], these two modes retain their characteristics in terms of frequencies and currents, while the impedances at resonance remain low [24]. The simulation allowed observing the variations of the currents and their relationship (Figure 5). The two loops are tuned to the same frequency f_0 = 105MHz, with k=0.05, L = 117.6nH, C = 19.47pF, R = 0.41Ω, and quality factor Q_0 = 189.

It can be seen that at f_o, the transfer of power from the primary to the secondary coil is optimal. This is a particularity of the inductive coupling which is widely used in RF [25-26]. For the other frequencies f_1 and f_2, the currents I_1 and I_2 have a maximum value and the difference between the two modes remains at the phase level.

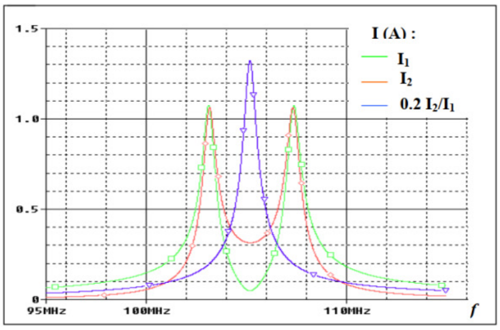

Fig. 5. I_1 and I_2 variation curves and their ratio.

V. EXPERIMENTAL RESULTS

A. *Prototype Dimensions*

The results of the experimental tests obtained with the developed coils are presented in this section. An ellipsoidal Helmholtz coil and a circular Helmholtz coil were built for MRI (H1) at 100.241MHz. To facilitate comparisons, they have the same radial size d=5cm. The precise dimensions of the coils are given in Table III. Figure 6 shows a photography of both developed coils. The diameter of the wire constituting the loops is 1mm.

TABLE III. COIL DIMENSIONS

Coils	Loop diameter	Distance between loops
Circular Helmholtz	5cm	2.5cm
Ellipsoidal Helmholtz	a=3cm, b=2.4cm	3.1cm

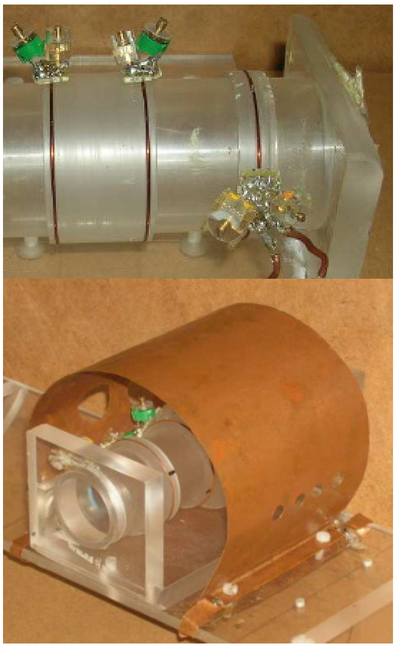

Fig. 6. Circular and ellipsoidal Helmholtz coils.

B. *Tuning and Matching of the Coils*

Each loop of the coil was tuned at the same self-resonance frequency f_0, higher than the resonance frequency of the coil. By predetermination of f_0, an empty preset of the coil can be accomplished. Fine tuning of the coil at the working frequency f_1 is then performed if necessary [27]. Using the HP 4195A network analyzer, we were able to obtain the variation of the magnitude and the phase in air without load of the input impedance seen by a test loop in terms of frequency as shown for the ellipsoidal coil in Figure 7.

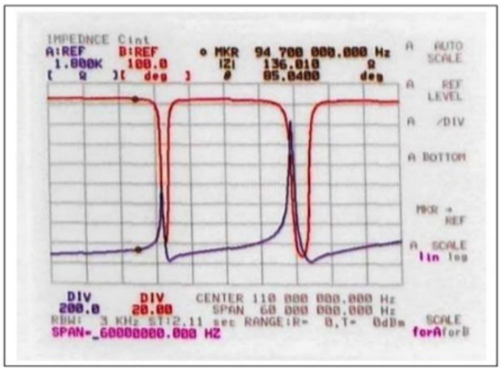

Fig. 7. Curve of the input impedance of the ellipsoidal coil seen by a test loop.

At resonance frequency f_1, there is almost the same value for the first mode and a small error for the second mode. At f_2, the difference is around 3% for the circular coil H_C and around 1% for the ellipsoidal coil H_E. The matching of the coils was carried out without load using a coupling loop (inductive coupling). The position of the coupling loop relatively to the coil determines the optimal distance to get an impedance of 50Ω for the matching [28]. This is approximately 1.9cm for the H_C (1.99cm in theory, this corresponds to an error of 5%) and 2.7cm for the H_E (2.56cm in theory, corresponding to an error of 6%). This matching technique allows optimal energy transfer between the coils and the transmission and reception system. It should be noted that the matching and tuning of the coils depend on the nature of the sample and therefore adjustments should be considered for any new load.

C. *Testing the Coils without Load*

Off-field (in-air) tests were performed for both H_C and H_E coils. Thus, in the absence of a sample, relative field measurements along the axis of the coils were carried out using a small measurement loop connected to the HP 4195A network analyzer, and comparative readings of the intensity profile of the magnetic field B_1 were established as shown in Figure 8. The experimental curves of the normalized magnetic induction produced along the Oz axis by both coils are given in Figure 9.

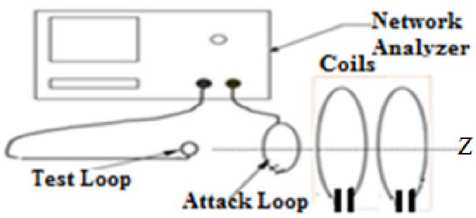

Fig. 8. Axial profiles in terms of distance (cm) for coils H_E and H_c.

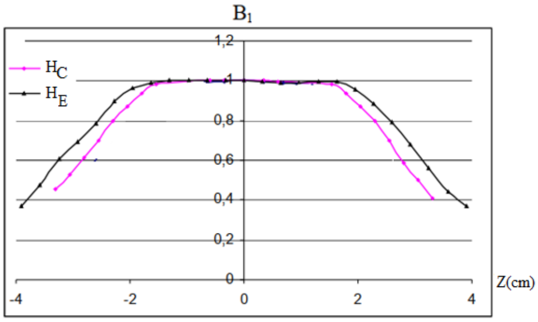

Fig. 9. Axial profiles in terms of distance (cm) for coils H_E and H_c.

The obtained B_1 field profiles along the axis for the two coils (Figure 8) are in good agreement with the theoretical predictions of Figure 2. Compared to the H_C (reference coil), the width at 10% of the lobe is 1.32 times greater for the ellipsoidal coil, which is comparable to the theoretical predictions. Another positive point for the ellipsoidal coil, its efficiency is better. Indeed, at identical absorbed power, the field emitted in the center is on average about 20% higher than that produced by the H_E coil. Moreover, the quality factor of the ellipsoidal coil has also an interesting increment of 32%.

VI. CONCLUSION

The design and testing of two prototype probes for MRI comprising two circular and ellipsoidal free elements was presented. The two loops are correctly spaced and connected directly in series to a tuning capacitor. A complete electrical modeling of the coils taking into account all couplings (inductive and capacitive) was investigated. For a given resonant frequency, a predetermination of the tuning frequency of the tuned circuits is carried out, as well as the calculation of the associated tuning capacitors.

At the practical level, the prototypes built are in fact of the same radial dimensions to facilitate comparisons. Thus, compared to the reference circular Helmholtz coil, field measurements in free space with the ellipsoidal coil are in good agreement with the theoretical predictions. The width of the lobe at 10% is increased by 20% for the ellipsoidal coil. Moreover, a significant improvement in the quality factor is observed in free space for the ellipsoidal coil. Also, the efficiency is increased by 37% for the ellipsoidal coil. Finally, the signal to noise ratio is higher for the ellipsoidal coil compared to the circular coil.

ACKNOWLEDGMENT

This research was supported by the Deanship of Scientific Research, Imam Mohammad Ibn Saud Islamic University, Saudi Arabia, Grant No. 2214114020.

REFERENCES

[1] F. Romeo and D. I. Hoult, "Magnet field profiling: Analysis and correcting coil design," *Magnetic Resonance in Medicine*, vol. 1, no. 1, pp. 44–65, 1984, https://doi.org/10.1002/mrm.1910010107.

[2] C. E. Hayes, W. A. Edelstein, J. F. Schenck, O. M. Mueller, and M. Eash, "An efficient, highly homogeneous radiofrequency coil for whole-body NMR imaging at 1.5 T," *Journal of Magnetic Resonance*, vol. 63, pp. 622–628, Jan. 1985, https://doi.org/10.1016/0022-2364(85)90257-4.

[3] J. T. Vaughan, H. P. Hetherington, J. O. Otu, J. W. Pan, and G. M. Pohost, "High frequency volume coils for clinical NMR imaging and spectroscopy," *Magnetic Resonance in Medicine*, vol. 32, no. 2, pp. 206–218, 1994, https://doi.org/10.1002/mrm.1910320209.

[4] K. Asher, N. K. Bangerter, R. D. Watkins, and G. E. Gold, "Radiofrequency Coils for Musculoskeletal MRI," *Topics in Magnetic Resonance Imaging*, vol. 21, no. 5, pp. 315–323, Oct. 2010, https://doi.org/10.1097/RMR.0b013e31823cd184.

[5] Q. X. Yang, S. H. Li, and M. B. Smith, "A Method for Evaluating the Magnetic Field Homogeneity of a Radiofrequency Coil by Its Field Histogram," *Journal of Magnetic Resonance, Series A*, vol. 108, no. 1, pp. 1–8, May 1994, https://doi.org/10.1006/jmra.1994.1081.

[6] K. Alsnaie, S. M. A. Ghaly, and M. A. Ali, "Study and Design of a Multi-range Programmable Sensor for Temperature Measurement," *Engineering, Technology & Applied Science Research*, vol. 12, no. 6, pp. 9601–9606, Dec. 2022, https://doi.org/10.48084/etasr.5284.

[7] S. M. A. Ghaly, K. A. Al-Snaie, M. O. Khan, M. Y. Shalaby, and M. T. Oraiqat, "Design and Simulation of an 8-Lead Electrical Capacitance Tomographic System for Flow Imaging," *Engineering, Technology & Applied Science Research*, vol. 11, no. 4, pp. 7430–7435, Aug. 2021, https://doi.org/10.48084/etasr.4122.

[8] S. M. A. Ghaly, K. A. Muhanna, and M. O. Khan, "Design and Testing of a Square Helmholtz Coil for NMR Applications with Relative Improved B1 Homogeneity," in *IEEE International Conference on Imaging Systems and Techniques*, Abu Dhabi, United Arab Emirates, Dec. 2019, pp. 1–6, https://doi.org/10.1109/IST48021.2019.9010469.

[9] S. M. A. Ghaly, M. O. Khan, K. Almuhanna, and K. A. Al-snaie, "A Free Element Spherical and Ellipsoidal Radio Frequency Coils with High B1 Homogeneity for MRI," in *IEEE International Conference on Imaging Systems and Techniques*, Abu Dhabi, United Arab Emirates, Dec. 2019, pp. 1–5, https://doi.org/10.1109/IST48021.2019.9010108.

[10] F. Alorifi, S. M. A. Ghaly, M. Y. Shalaby, M. A. Ali, and M. O. Khan, "Analysis and Detection of a Target Gas System Based on TDLAS & LabVIEW," *Engineering, Technology & Applied Science Research*, vol. 9, no. 3, pp. 4196–4199, Jun. 2019, https://doi.org/10.48084/etasr.2736.

[11] S. M. A. Ghaly, K. A. Al-Snaie, and A. M. Ali, "Design and Modeling of a Radiofrequency Coil Derived from a Helmholtz Structure," *Engineering, Technology & Applied Science Research*, vol. 9, no. 2, pp. 4037–4043, Apr. 2019, https://doi.org/10.48084/etasr.2683.

[12] S. M. A. Ghaly, "LabVIEW Based Implementation of Resistive Temperature Detector Linearization Techniques," *Engineering, Technology & Applied Science Research*, vol. 9, no. 4, pp. 4530–4533, Aug. 2019, https://doi.org/10.48084/etasr.2894.

[13] S. M. A. Ghaly and M. O. Khan, "Design, Simulation, Modeling, and Implementation of a Square Helmholtz Coil in Contrast with a Circular Coil for MRI Applications," *Engineering, Technology & Applied Science Research*, vol. 9, no. 6, pp. 4990–4995, Dec. 2019, https://doi.org/10.48084/etasr.3171.

[14] S. Li, Q. X. Yang, and M. B. Smith, "RF coil optimization: Evaluation of B1 field homogeneity using field histograms and finite element calculations," *Magnetic Resonance Imaging*, vol. 12, no. 7, pp. 1079–1087, Jan. 1994, https://doi.org/10.1016/0730-725X(94)91240-W.

[15] B. Gruber, M. Froeling, T. Leiner, and D. W. J. Klomp, "RF coils: A practical guide for nonphysicists," *Journal of Magnetic Resonance Imaging*, vol. 48, no. 3, pp. 590–604, 2018, https://doi.org/10.1002/jmri.26187.

[16] J. Mispelter, M. Lupu, and A. Briguet, *NMR Probeheads for Biophysical and Biomedical Experiments: Theoretical Principles & Practical Guidelines*. London, UK: Imperial College Press, 2006.

[17] B. J. Dardzinski, S. Li, C. M. Collins, G. D. Williams, and M. B. Smith, "A Birdcage Coil Tuned by RF Shielding for Application at 9.4 T," *Journal of Magnetic Resonance*, vol. 131, no. 1, pp. 32–38, Mar. 1998, https://doi.org/10.1006/jmre.1997.1334.

[18] S. M. Ahmed Ghaly and S. Al-Sowayan, "A High B1 Field Homogeneity Generation Using Free Element Elliptical Four-Coil System," *American Journal of Applied Sciences*, vol. 11, no. 4, pp. 534–540, Feb. 2014, https://doi.org/10.3844/ajassp.2014.534.540.

[19] S. M. A. Ghaly, K. A. Al-snaie, and S. S. Al-Sowayan, "Design and Testing of Radiofrequency Spherical four Coils," *Modern Applied Science*, vol. 10, no. 5, pp. 186–186, 2016.

[20] S. M. Ahmed Ghaly, K. Al-Snaie, and M. Khan, "Spherical and Improved Helmholtz Coil with High B1 Homogeneity for Magnetic Resonance Imaging," *American Journal of Applied Sciences*, vol. 13, no. 12, pp. 1413–1418, Dec. 2016, https://doi.org/10.3844/ajassp.2016.1413.1418.

[21] J. Wang, S. She, and S. Zhang, "An improved Helmholtz coil and analysis of its magnetic field homogeneity," *Review of Scientific Instruments*, vol. 73, no. 5, pp. 2175–2179, Apr. 2002, https://doi.org/10.1063/1.1471352.

[22] M. Decorps, P. Blondet, H. Reutenauer, J. P. Albrand, and C. Remy, "An inductively coupled, series-tuned NMR probe," *Journal of Magnetic Resonance*, vol. 65, no. 1, pp. 100–109, Oct. 1985, https://doi.org/10.1016/0022-2364(85)90378-6.

[23] J. Murphy-Boesch and A. P. Koretsky, "An in Vivo NMR probe circuit for improved sensitivity," *Journal of Magnetic Resonance*, vol. 54, no. 3, pp. 526–532, Oct. 1983, https://doi.org/10.1016/0022-2364(83)90333-5.

[24] R. F. Lee, R. O. Giaquinto, and C. J. Hardy, "Coupling and decoupling theory and its application to the MRI phased array," *Magnetic Resonance in Medicine*, vol. 48, no. 1, pp. 203–213, 2002, https://doi.org/10.1002/mrm.10186.

[25] C. M. Collins and Z. Wang, "Calculation of radiofrequency electromagnetic fields and their effects in MRI of human subjects," *Magnetic Resonance in Medicine*, vol. 65, no. 5, pp. 1470–1482, 2011, https://doi.org/10.1002/mrm.22845.

[26] Y. E. Esin and F. N. Alpaslan, "MRI image enhancement using Biot-Savart law at 3 tesla," *Turkish Journal of Electrical Engineering and Computer Sciences*, vol. 25, no. 4, pp. 3381–3396, Jan. 2017, https://doi.org/10.3906/elk-1604-348.

[27] D. M. Ginsberg and M. J. Melchner, "Optimum Geometry of Saddle Shaped Coils for Generating a Uniform Magnetic Field," *Review of Scientific Instruments*, vol. 41, no. 1, pp. 122–123, Nov. 2003, https://doi.org/10.1063/1.1684235.

[28] H. Fujita, T. Zheng, X. Yang, M. J. Finnerty, and S. Handa, "RF Surface Receive Array Coils: The Art of an LC Circuit," *Journal of Magnetic Resonance Imaging*, vol. 38, no. 1, pp. 12–25, 2013, https://doi.org/10.1002/jmri.24159.